# Characterization of $(NH_3)_{n=1-6}NH^+$ Clusters Produced by $^{252}Cf$ Fragments Impact onto a $NH_3$ Condensed Target

**Francisco Alberto Fernandez-Lima,[†,‡] Thiago Messias Cardozo,[‡] R. M. Rodriguez,[†] Cássia Ribeiro Ponciano,[†] Enio Frota da Silveira,[†] and Marco Antonio Chaer Nascimento*[,‡]**

*Physics Department, Pontifícia Universidade Católica, Rua Marques de São Vicente 225, Rio de Janeiro 22542-900, Brazil, and Instituto de Química, Universidade Federal do Rio de Janeiro, Rio de Janeiro 21949-900, Brazil*

*Received: May 17, 2007; In Final Form: June 19, 2007*

This paper reports the first characterization of the $(NH_3)_nNH^+$ cluster series produced by a $^{252}Cf$ fission fragments (FF) impact onto a $NH_3$ ice target. The $(NH_3)_{n=1-6}NH^+$ members of this series have been analyzed theoretically and experimentally. Their ion desorption yields show an exponential dependence of the cluster population on its mass, presenting a relative higher abundance at $n = 5$. The results of DFT/B3LYP calculations show that two main series of ammonium clusters may be formed. Both series follow a clear pattern: each additional $NH_3$ group makes a new hydrogen bond with one of the hydrogen atoms of the respective $\{NH_3\text{-}NH\}^+$ and $\{NH_2NH_2\}^+$ cores. The energy analysis (i.e., *D*-plot and stability analysis) shows that the calculated members of the $(NH_3)_{n-1}\{NH_2NH_2\}^+$ series are more stable than those of the $(NH_3)_{n-1}\{NH_3NH\}^+$ series. The trend on the relative stability of the members of more stable series, $(NH_3)_{n-1}\{NH_2NH_2\}^+$, shows excellent agreement with the experimental distribution of cluster abundances. In particular, the $(NH_3)_4\{NH_2NH_2\}^+$ structure is the most stable one, in agreement with the experiments.

## 1. Introduction

Studies on the structure and properties of cluster ions in the gas phase have been conducted for many decades. Investigation on the formation of ammonia or water clusters are of particular interest since they provide insight into the nature of hydrogen-bonded systems not only in the gaseous state but also in the liquid and solid phases. Recently, several theoretical and experimental investigations on hydrogen-bonded molecular clusters of polar molecules, especially water and ammonia containing clusters, have been reported.[1−15] The generation of positively charged ammonia clusters has been performed using a number of different ionization techniques: multiphoton ionization,[16−18] single-photon ionization,[19] electron impact ionization,[20−22] and ultrafast pump−probe techniques.[23−25] The main positively charged ammonia cluster series observed experimentally are as follows: $(NH_3)_nNH_2^+$, $(NH_3)_nNH_3^+$, $(NH_3)_nNH_5^+$, $(NH_3)_nNH_4^+$, the last one being the predominant one.

The study of such series, produced by electronically induced sputtering on low-temperature condensed-gas solids (ices) [e.g., refs 26−30] is important for understanding cometary surfaces and outer-solar-system atmospheres.[31−33] In a recent paper, the generation of ammonia cluster ions (positive and negative) performed via the impact of highly energetic and highly charged fission fragments (FF) from a $^{252}Cf$ source on the $NH_3$ ice surface at controlled temperature was reported.[34] Different from the previous experiments using other ionization techniques, the technique employed in ref 34 gives rise to a new series of clusters $(NH_3)_{1-6}NH^+$ in addition to the ones previously reported.

From the theoretical side, with the advent of predictive ab initio methods, cluster ions have been investigated with several methodologies including accurate ab initio methods that include electron correlation. Ab initio calculations on ammonia clusters have been extensively performed using the Hartree−Fock (HF) method,[22,35] the Møller-Plesset (MP) perturbation theory,[22,36−38] the coupled cluster (CC) methods,[36,38,39] and the density functional theory (DFT) with extended basis. In a previous paper, DFT calculations with extended basis were used to explain the relative mass abundance of $(NH_3)_{1-8}NH_4^+$ and $(NH_3)_{1-8}NH_2^-$ ammonia clusters (magic numbers).[40,41] The calculations have shown that the clusters' stability can be related to the magic numbers observed in the mass spectra.[40,41]

Although studies on positively and negatively charged ammonia clusters have been reported, to our knowledge a comprehensive and detailed characterization of the $(NH_3)_{1-6}NH^+$ series has not been performed. This paper reports the first characterization of the $(NH_3)_{1-6}NH^+$ cluster series produced by a $^{252}Cf$ fission fragment (FF) impact onto a $NH_3$ ice target. In particular, we are interested in describing the correlation between the cluster stability and the relative cluster populations in the mass spectra. The observed results are discussed based on a systematic search for the more stable conformers using density functional theory at the B3LYP level of calculation with extended basis set.

## 2. Experimental Methods

The experimental details of the $^{252}Cf$-PDMS technique can be found elsewhere.[26−29,34,42] Briefly, an $NH_3$ ice target is grown by condensation of $NH_3$ gas over an Au substrate at low and controlled temperature. Fission fragments from a $^{252}Cf$ source are impacted onto the $NH_3$ ice target, inducing desorption of positive and negative ions, as well as of neutral particles, at high-vacuum conditions ($10^{-9}$ mbar). The desorbed ions are

* To whom correspondence should be addressed. E-mail: chaer@iq.ufrj.br.
† Pontifícia Universidade Católica.
‡ Universidade Federal do Rio de Janeiro.

10.1021/jp073827p CCC: $37.00 
Published on Web 08/08/2007 PAGE EST: 5.1

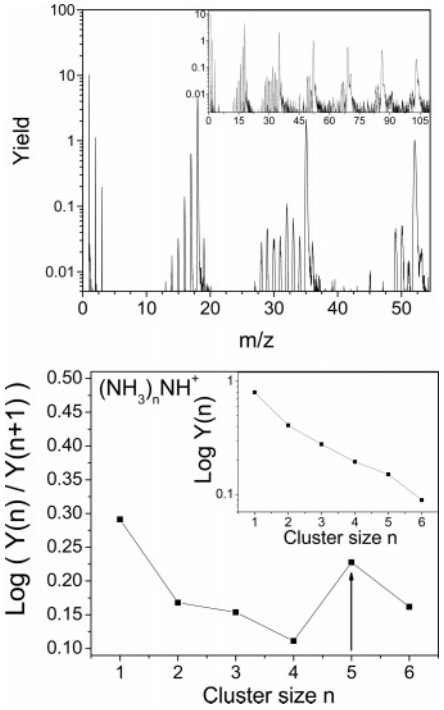


**Figure 1.** (a) Time-of-flight mass spectrum of the $NH_3$ ice bombarded by $^{252}Cf$ fission fragments. The inset is an extension of the spectrum for *m* up to ~105 u. (b) Relative secondary ion yields of the $(NH_3)_n$-$NH^+$ series as a function of the number of $NH_3$ units. The inset shows the exponential decrease of the $(NH_3)_nNH^+$ yield as a function of the number of $NH_3$ units.

accelerated by an extraction field toward the drift region and are detected by a secondary ion detector. Mass analysis is performed by time-of-flight technique (TOF).[43] A correction has been applied to take into account that the detection efficiency of the ionized clusters varies smoothly and monotonically across the mass range. The typical mass-resolution power in the current spectra is about $m/\Delta m \sim 200$ for the worst case. Nevertheless, even within such a modest resolution, the peaks are completely resolved for low values of *n*.

The $^{252}Cf$ FF impact produces secondary ions whose structure can be written as $(NH_3)_nNH_m^+$, where $m = 1-5$ (Figure 1 top). The desorption yields $Y(n)$ of the members of the $(NH_3)_{n=1-6}NH^+$ series decrease exponentially as a function of the cluster size: $Y(n) \sim \exp(-0.178n)$. A relative higher abundance is observed for the cluster $(NH_3)_{n=5}NH^+$ compared to the other members of this series (Figure 1 bottom).

### 3. Theoretical and Computational Details

Theoretical calculations have been performed, at the B3LYP/6-311G** level, with the purpose of determining the most stable structures of the $(NH_3)_{n=1-7}NH^+$ ammonia clusters and to investigate if the clusters stability could be directly related to their relative cluster populations in the mass spectra. The basis set superposition error was found to be of the order of 0.02 eV. A vibration analysis was performed for all the obtained structures at the level of calculation employed. All frequencies were found to be real, indicating that the optimized structures correspond to true minima in the potential energy hypersurfaces. The frequencies were also used to compute the zero-point correction energy (ZPE) for all the optimized structures. No symmetry restrictions or those of any other kind have been imposed in the process of geometry optimization.

It is well-known that DFT calculations on charged species may be in error due to the fact that, for most of the present

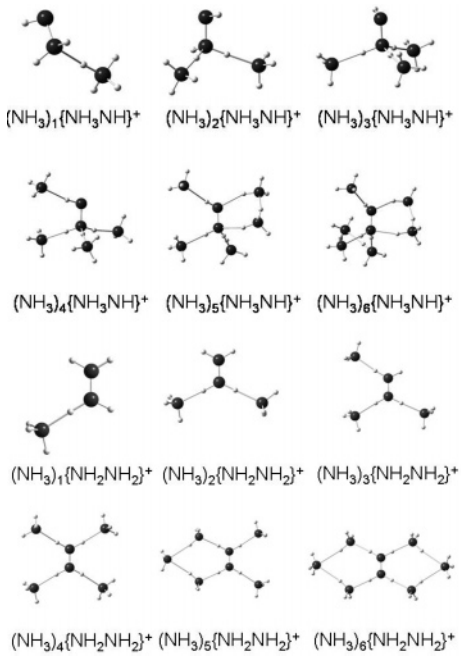


**Figure 2.** Optimized geometries of the $(NH_3)_{n-1}\{NH_3NH\}^+$ and $(NH_3)_{n-1}\{NH_2NH_2\}^+$ series at the DFT/B3LYP/6-311G** level of calculation.

available functionals, the exchange energy does not exactly cancel the Coulombic self-interaction.[44] On the other hand, this effect becomes less important as the size of the ions increase. To check for possible inconsistencies, the smaller structures were also optimized at the MP2/ 6-311G** level of calculation. No substantial changes were observed either in the geometrical parameters or in the relative stability of the clusters.

The barrier for the interconversion between the two different $N_2H_4^+$ cores was also determined, taking into account the zero-point energy correction. A vibration analysis confirmed that both cores optimized geometries correspond to minima in their potential energy surfaces and that the optimized transition state geometry is a first-order saddle point. An intrinsic reaction coordinate (IRC) was performed to verify that the determined transition state does connect the two core structures.

All calculations were carried out using the Jaguar 6.0 software package.[45]

### 4. Results and Discussion

The systematical search for the most stable structures shows that two main series of ammonium clusters can be produced (Figure 2), corresponding to two distinct $N_2H_4^+$ central cores, $\{NH_3NH\}^+$ and $\{NH_2NH_2\}^+$, to which the $NH_3$ units are attached. The similarity of the obtained structures suggests that the mechanism of the cluster formation is strongly related to the formation of the ion cores and the successive attachments of $NH_3$ neutral units. The charge distribution of the cores were found to be $(NH_3)^{0.11+}NH^{0.89+}$ and $NH_2^{0.5+}NH_2^{0.5+}$.

**Ion Core Formation.** The ion core formation can be described by the following:

Channel A:

$$NH_3^0 + NH^+ \rightarrow \{NH_3NH\}^+;$$
$$\Delta E = -6.59 \text{ eV}; \Delta G = -6.25 \text{ eV}$$

Channel B:

$$NH_3^+ + NH^0 \rightarrow \{NH_3NH\}^+; \quad \Delta E = -5.25 \text{ eV}; \Delta G = -4.92 \text{ eV}$$

Channel C:

$$NH_2 + NH_2^+ \rightarrow \{NH_2NH_2\}^+; \quad \Delta E = -7.50 \text{ eV}; \Delta G = -7.11 \text{ eV}$$

Channel D*:

$$NH_3^+ + NH^0 \rightarrow \{NH_3NH\}^{+}* \rightarrow \{NH_2NH_2\}^+; \quad \Delta E = -6.62 \text{ eV}; \Delta G = -7.62 \text{ eV}$$

Channel E*:

$$NH_3^0 + NH^+ \rightarrow \{NH_3NH\}^{+}* \rightarrow \{NH_2NH_2\}^+; \quad \Delta E = -7.96 \text{ eV}; \Delta G = -6.29 \text{ eV}$$

All the thermodynamic properties were calculated at the DFT/B3LYP/6-311G** level considering a temperature of 298.15 K. The $\Delta G$ values indicate that all of the described channels are thermodynamically favorable. However, the channels have different rates, depending on the production efficiency, ionization efficiency, and stability of the reactant molecules. The analysis of the experimental and the theoretical results can provide some insights on the mechanism of the ion core formation.

The relative experimental ion desorption yields are $Y(NH^+)$:$Y(NH_2^+)$:$Y(NH_3^+)$ = 1:3.8:18.2. The ion desorption by fast projectiles (~50 MeV) is characterized by a high emission of neutral species, and an estimated ~1% emission of ionic species.[29] Moreover, if one assumes that the neutral species formation follow the same trend as the ionic ones [$Y(NH^0)$:$Y(NH_2^0)$:$Y(NH_3^0)$], the probability of formation of each core structure can be estimated. Since the ion yields are directly related to the probability of the ion formation, then the relative probability of channels A−C can be described as

$$P(\text{Channel A}):P(\text{Channel B}):P(\text{Channel C}) = Y(NH_3^0)Y(NH^+):Y(NH_3^+)Y(NH^0):Y(NH_2^0)Y(NH_2^+)$$

or

$$P(\text{Channel A}):P(\text{Channel B}):P(\text{Channel C}) = 18.2:18.2:14.44$$

The higher probability of channels A and B is related to the structure of the $NH_3$ ice target, which makes the $NH_3^0$ species the most probable emitted fragments. Nevertheless, the $Y(NH^+)$:$Y(NH_2^+)$:$Y(NH_3^+)$ ratio is also affected by whether these ions are formed directly from the surface or from the fragmentation of larger emitted species.

The D* and E* channels are characterized by a two-step process: (i) the formation of the $\{NH_3NH\}^{+}*$ and (ii) its conversion to $\{NH_2NH_2\}^+$. The first step has the same probability as the A and B channels. However, the transformation of the $\{NH_3NH\}^{+}*$ core structure into $NH_2NH_2^+$ depends on the energy barrier for this process (Figure 3). The calculated barrier to convert $(NH_3)NH^+$ into $NH_2NH_2^+$ is 1.61 eV, and the barrier for the reverse process is 2.98 eV. The large amount of energy required for the interconvertion of one core structure into the other makes these processes unlikely to occur. Thus, once formed, the cores should retain their original structures.

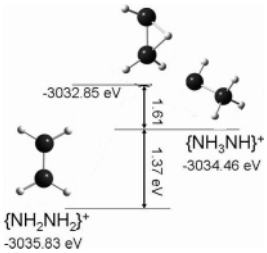


**Figure 3.** Mechanism of interconvertion between the two proposed core structures.

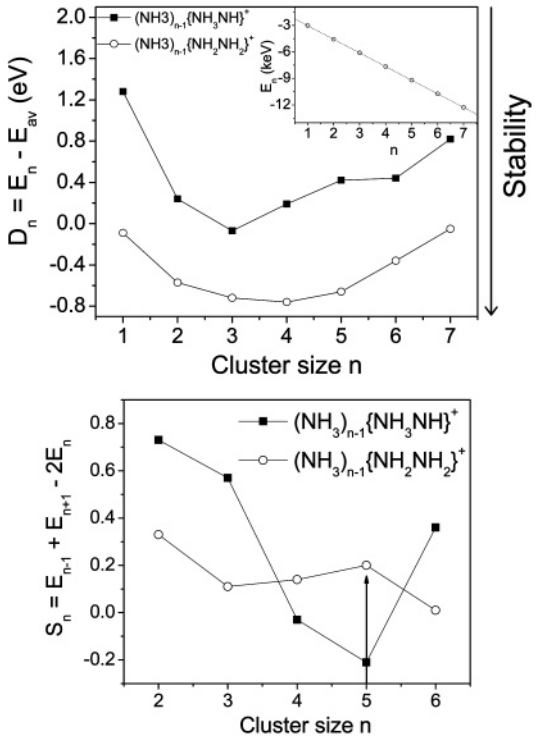


**Figure 4.** (top) *D*-plot: Deviation of the total cluster energy as a function of the cluster size *n*. In the inset, the total energy $E_n$ as a function of the cluster size. (bottom) Theoretical clusters stability as a function of the cluster size *n*. Data are given in Table 2.

**Deviation Plot Analysis (*D*-Plot).** The obtained structures can be classified by their conformational similarities or, as previously proposed,[40,41] by their total internal energy. The taxonomic exercise consists of logically conciliating these different types of sorting. Let $E_n(i)$ be the total energy of the *i*th isomer of the $(NH_3)_{n=1-6}NH^+$ cluster and $E_{av}((NH_3)_{n=1-6}NH^+)$ the average energy of all *n*-isomers. The average energy shows a linear dependence on *n*, as depicted in the inset of Figure 4 (top): $E_{av}((NH_3)_{n=1-6}NH^+) = -1496.44 - 1539.30n$. For each isomer, the deviation energy *D* is defined as $D_n(i) \equiv E_n(i) - E_{av}((NH_3)_{n=1-6}NH^+)$ so that the smaller the *D* value, the lower the energy of the isomer and the more stable it is. The relevant aspect of the *D*-plot is that certain isomers present the same systematic deviation, revealing the successive attachment of the same molecular unit.

As previously discussed,[40,41] from the *D*-plot one sees the following: (i) the cluster series can be characterized by their *D* behavior; (ii) for a given cluster size *n*, the *D*-plot shows the relative stability of the possible isomers; and (iii) for a given series, the successive *D* value differences (stability function, see next section) indicate the relative cluster stability of the different isomers. The series stability is well-described by the

**TABLE 1: Theoretical Results for the Clustering of Ammonia around the $\{NH_3NH\}^+$ and $\{NH_2NH_2\}^+$ Cations at the B3LYP/6-311G** Level of Calculation[a]**

| cluster size | DFT energy $E_n$ (eV) | | binding energy BE (eV) | |
|---|---|---|---|---|
| $n$ | $(NH_3)_{n-1}$ $\{NH_3NH\}^+$ | $(NH_3)_{n-1}$ $\{NH_2NH_2\}^+$ | $(NH_3)_{n-1}$ $\{NH_3NH\}^+$ | $(NH_3)_{n-1}$ $\{NH_2NH_2\}^+$ |
| 1 | −3034.46 | −3035.83 | 6.59 | 7.96 |
| 2 | −4574.80 | −4575.61 | 1.75 | 1.19 |
| 3 | −6114.41 | −6115.06 | 1.02 | 0.86 |
| 4 | −7653.45 | −7654.40 | 0.45 | 0.75 |
| 5 | −9192.52 | −9193.60 | 0.48 | 0.61 |
| 6 | −10731.80 | −10732.60 | 0.69 | 0.41 |
| 7 | −12270.72 | −12271.59 | 0.33 | 0.40 |

[a] $E(NH_3) = -1538.59$ eV at the DFT/B3LYP/6-311G** level. Binding energies calculated according to the equation BE $= E_{n-1} + E(NH_3) - E_n$.

*D*-plot analysis: the members of the $(NH_3)_{n-1}\{NH_2NH_2\}^+$ series present lower energy values than those of the $(NH_3)_{n-1}\{NH_3NH\}^+$ series.

**Stability Analysis.** The cluster stability can be related to two quantities: the binding energy (BE, as defined below) and the cluster geometry (size of the solvation shell), which are, of course, closely related. The binding energies (BE) were calculated considering the reactions

$$(NH_3)_{n-1}\{NH_3NH\}^+ \rightarrow (NH_3)_{n-2}\{NH_3NH\}^+ + NH_3 \quad (1)$$

$$(NH_3)_{n-1}\{NH_2NH_2\}^+ \rightarrow (NH_3)_{n-2}\{NH_2NH_2\}^+ + NH_3 \quad (2)$$

The energy of the clusters, including ZPE, and the binding energies are shown in Table 1.

Both the energy values and the *D*-plot analysis show that the members of the $(NH_3)_{n-1}\{NH_2NH_2\}^+$ series are more stable than the ones of the $(NH_3)_{n-1}\{NH_3NH\}^+$ one. The binding in both series is essentially due to electrostatic forces. The $(NH_3)NH^+$ and $NH_2NH_2^+$ cores polarize the $NH_3$ neutral units, resulting in a net attractive force that binds these units to the central core. The closer the $NH_3$ unit is to core, the stronger the attractive force should be. However, as the number of $NH_3$ units increases, steric effects start to play a role in determining how close from the central core these units can be. The contribution of steric effects can be inferred from the trend in the BE values as the cluster size increases. On the other hand, for the larger clusters, the attraction from the central core and the mutual polarization between the ligands may lead to larger BE values as in the case of the $(NH_3)_5\{NH_3NH\}^+$ and $(NH_3)_6\{NH_3NH\}^+$structures.

The stability analysis was performed using the commonly defined stability function $S_n = E_{n-1} + E_{n+1} - 2E_n$, where $E$ is the total energy of the corresponding cluster, including the zero point correction energy ($E = E_t + \text{ZPE}$). The relative stability of the clusters is a function of the charge stabilization provided by the $NH_3$ ligands and of the arrangement of these ligands around the central core as to minimize the steric repulsion among them.

**$(NH_3)_{n-1}\{NH_2NH_2\}^+$ Series.** Considering that the time scale of the TOF experiment ($\sim 10^{-6}$ s) is much larger than the time elapsed since the ionic cluster formation and its reorganization and fragmentation ($\sim 10^{-14}-10^{-13}$ s), it is quite reasonable to assume that the species being detected (the ones formed during time interval of $\sim 10^{-8}-10^{-7}$ s) are the thermodynamically more stable.

The stability trend of the $(NH_3)_{n-1}\{NH_2NH_2\}^+$ series agrees with that obtained from the experimental data, the $(NH_3)_{n=5}$-$NH^+ \leftrightarrow (NH_3)_4\{NH_2NH_2\}^+$ being the most stable cluster of this series (Figures 1 and 4). For the $(NH_3)_{n-1}NH_2NH_2^+$ series, it is clear that $n = 5$ is the maximum number of $NH_3$ units that can be attached to the central $NH_2NH_2^+$ core providing the lowest steric repulsion among the ligands. Therefore, it should the most stable one (Table 2). The distance from the $NH_3$ units to the central core (center of mass of the core) shows an almost constant value for $n$ up to 5 (Figure 5). Further addition of $NH_3$ units opens the second solvation shell, the additional $NH_3$ units being attached to the terminal hydrogen atoms of one of the $NH_3$ units of the first solvation shell. The second solvation shell should be completed at $n = 15$ ($n-1 = 14$), after which a third solvation shell should start to be filled, probably according to the same mechanism.

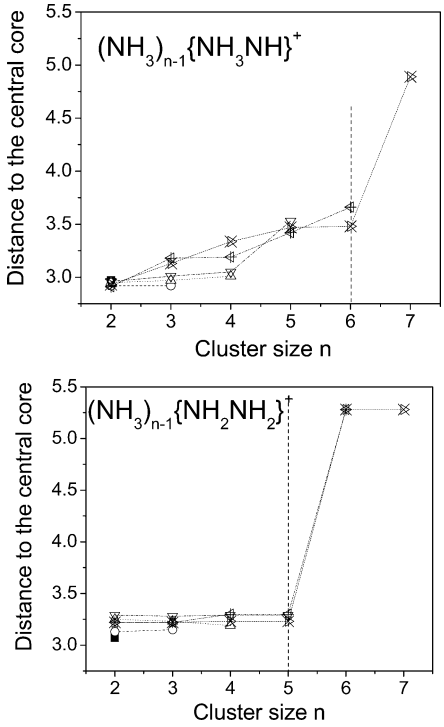


**Figure 5.** Distances from the $NH_3$ units to the center of mass of the core.

**TABLE 2: Experimental Yield $Y(n)$ and Theoretical Stability ($S_n$) Values**

| cluster size | experimental yield | | $S_n = E_{n-1} + E_{n+1} - 2E_n$ (eV) | |
|---|---|---|---|---|
| $n$ | $Y(n)$ | Log($Y(n)$/ $Y(n+1)$) | $(NH_3)_{n-1}$ $\{NH_3NH\}^+$ | $(NH_3)_{n-1}$ $\{NH_2NH_2\}^+$ |
| 1 | 0.799 | 0.291 | | |
| 2 | 0.409 | 0.168 | 0.73 | 0.33 |
| 3 | 0.277 | 0.154 | 0.57 | 0.11 |
| 4 | 0.195 | 0.111 | −0.03 | 0.14 |
| 5 | 0.151 | 0.228 | −0.21 | 0.2 |
| 6 | 0.089 | 0.162 | 0.36 | 0.01 |
| 7 | 0.061 | | | |

Figure 6 shows the core charge for the $\{NH_3NH\}^+$ and $\{NH_2$-$NH_2\}^+$ species, computed by fitting of the electrostatic potential using the CHelpG algorithm,[46] as a function of the cluster size. For both series the core charge decreases as the cluster size increases. Moreover, the charge of the $\{NH_2NH_2\}^+$ is always higher than that of the $\{NH_3NH\}^+$ core. This higher charge certainly contributes to the higher stability of the $(NH_3)_{n-1}NH_2NH_2^+$ series.

**$(NH_3)_{n-1}\{NH_3NH\}^+$ Series.** The $(NH_3)_{n-1}\{NH_3NH\}^+$ series shows a very different trend from that observed in the experimental data (Figures 1 and 4). The stability of this series

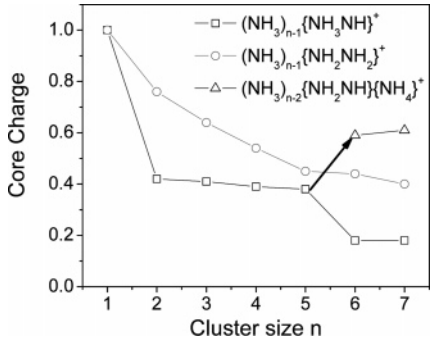


**Figure 6.** Core charge as a function of the cluster size.

decreases as a function of the cluster size, presenting a minimum value at $(NH_3)_{n=5}NH^+ \leftrightarrow (NH_3)_4\{NH_3NH\}^+$. The distance of the $NH_3$ units to the central core (center of mass of the core) shows a large increase after $n = 6$, defining the first solvation shell (Figure 5). Similarly to the other series, further addition of $NH_3$ units opens the second solvation shell, with the additional $NH_3$ units being attached to the terminal hydrogen atoms of one of the $NH_3$ units of the first solvation shell. The relative higher stability at $n = 6$ observed in the *D*-plot and in the stability analysis is consistent with the completion of the first solvation shell, when the maximum number of $NH_3$ units are attached to the $\{NH_3NH\}^+$ central core. However, the relative higher stability observed for $n = 6$; i.e., $(NH_3)_{n=6}NH^+ \leftrightarrow (NH_3)_5\{NH_3NH\}^+$ structure is not evident from the shell analysis. The large stability of this cluster is a consequence of a charge redistribution such that a $NH_4^+$ unit becomes the cluster core (Figure 6). This change in the nature of the core, observed at $n = 6$, implies that the $n = 6$ and 7 members of the $(NH_3)_{n-1}\{NH_3NH\}^+$ series should be more appropriately denoted as $(NH_3)_{n-2}\{NH_2NH\}\{NH_4\}^+$. Therefore, when comparing the relative stabilities of the clusters with $n < 6$ and $n \geq 6$, one should take into account the fact that they belong to different series (different cores).

## 5. Conclusions

The $(NH_3)_{n=1-6}NH^+$ clusters produced by $^{252}CF$ impact onto a $NH_3$ condensed target have been analyzed theoretically and experimentally. The desorption yields show an exponential dependence of the cluster population on its mass, revealing a relative higher abundance (special stability) at $n = 5$.

The DFT/B3LYP calculations show that two main series of ammonium clusters can be produced. Similar results are obtained at the MP2 level of calculation for the smaller structures. Both series follow a clear pattern: each additional $NH_3$ group makes a new hydrogen bond with one of the hydrogen atoms of the respective $\{NH_3NH\}^+$ and $\{NH_2NH_2\}^+\}$ cores.

The *D*-plot analysis shows that the obtained structures can be classified by their conformational similarities or, within a better taxonomical description, by their total internal energy. The energy analysis indicate that the members of the $(NH_3)_{n-1}\{NH_2NH_2\}^+$ series are more stable than those of the $(NH_3)_{n-1}\{NH_3NH\}^+$ series. The trend on the relative stability of the more stable series, $(NH_3)_{n-1}\{NH_2NH_2\}^+$, presents excellent agreement with the experimental distribution of cluster abundances, with the $(NH_3)_4\{NH_2NH_2\}^+$ structure being the most stable one. This agreement is probably due to the fact that the time scale of the TOF experiment ($\sim 10^{-6}$ s), being much larger than the time for the clusters formation, reorganization, and fragmentation ($\sim 10^{-14}$-$10^{-13}$ s), favors the detection of the thermodynamically more stable clusters. The core charges and the shell analysis are also consistent with the energetic analysis.

IRC calculations show that the energy barriers are high enough to prevent the interconversion of one core structure into the other. This is probably the reason why the series contribution to the mass spectra is well-described by the results of the stability analysis using the more stable structures.

**Acknowledgment.** The authors would like to acknowledge the Brazilian Agencies CNPq, Faperj, and CLAF for their support.

## References and Notes

(1) Kryachko, E. S. *Chem. Phys. Lett.* **1997**, *272*, 132.
(2) Kim, J.; Majumbar, D.; Lee, H. M.; Kim, K. S. *J. Chem. Phys.* **1999**, *110*, 9128.
(3) Sadlej, J.; Kzimirski, J. K.; Buck, U. *J. Phys. Chem. A* **1999**, *103*, 9128.
(4) Smith, D. M. A.; Smets, J.; Elkadi, A.; Adamowics, L. *J. Chem. Phys.* **1998**, *109*, 1238.
(5) Kulkarni, S. A.; Bartolotti, L. J.; Pathak, R. K. *J. Chem. Phys.* **2000**, *113*, 2697.
(6) Pawlowski, P. M.; Okimoto, S. R.; Tao, F. M. *J. Phys. Chem. A* **2003**, *107*, 5327.
(7) Antolovich, M.; Lindoy, L. F.; Reimers, J. R. *J. Phys. Chem. A* **2004**, *108*, 8434.
(8) Sadlej, J.; Moszynski, M.; Doborowolski, J. Cz.; Mazurek, A. P. *J. Phys. Chem. A* **1999**, *103*, 8529.
(9) Armunanto, R.; Schwenk, C. F.; Rode, B. M. *J. Phys. Chem. A* **2005**, *109*, 4437.
(10) Lenz, A.; Ojamae, L. *Phys. Chem. Chem. Phys.* **2005**, *7*, 1905.
(11) Schulz, F.; Hartke, B. *Phys. Chem. Chem. Phys.* **2003**, *5*, 5021.
(12) Sobolewski, A. L.; Domcke, W. *Phys. Chem. Chem. Phys.* **2005**, *7*, 970.
(13) Farenzena, L. S.; Martinez, R.; Iza, P.; Ponciano, C. R.; Homen, M. G. P.; Naves de Brito, A.; da Silveira, E. F.; Wien, K. *Int. J. Mass Spectrom.* **2006**, *255*, 1.
(14) Odutola, J. A.; Dyke. T. R.; Howard, B.; Muether, J. S. *J. Chem. Phys.* **1979**, *70*, 4884.
(15) Süzer, S.; Andrews, L. *J. Chem. Phys.* **1987**, *87*, 5131.
(16) Wei, S.; Kilgore, K.; Tzeng, W. B.; Castleman, A. W., Jr. *J. Chem. Phys.* **1990**, *92*, 332.
(17) Wei, S.; Kilgore, K.; Tzeng, W. B.; Castleman, A. W., Jr. *J. Chem. Phys.* **1990**, *93*, 2506.
(18) Wei, S.; Kilgore, K.; Tzeng, W. B.; Castleman, A. W., Jr. *J. Chem. Phys.* **1991**, *95*, 8306.
(19) Shinohara, H.; Nishi, N.; Washida, N. *J. Chem. Phys.* **1985**, *83*, 1939.
(20) Peifer, W. R.; Coolbaugh, M. T.; Garvey, J. F. *J. Chem. Phys.* **1989**, *91*, 6684.
(21) Lifshitz, C.; Louage, F. *J. Phys. Chem.* **1989**, *93*, 5635.
(22) Ichihashi, M.; Yamabe, J. Y.; Muray, K.; Nonose, S.; Hirao, K.; Kondow, T. *J. Phys. Chem.* **1996**, *100*, 10050.
(23) Card, D. A.; Folmer, D. E.; Sato, S.; Buzza, S. A.; Castleman, A. W., Jr. *J. Phys Chem. A* **1997**, *101*, 3417.
(24) Freudenberg, T.; Stert, V.; Radloff, W.; Ringling, J.; Güddle, J.; Korn, G.; Hertel, V. *Chem. Phys. Lett.* **1997**, *269*, 523.
(25) Wei, S.; Purnell, J.; Buzza, S. A.; Stanley, R. J.; Castleman, A. W., Jr. *J. Chem. Phys.* **1992**, *97*, 9480.
(26) Farenzena, L. S.; Iza, P.; Martinez, R.; Fernandez-Lima, F. A.; Seperuelo, E. D.; Faraudo, G. S.; Ponciano, C. R.; Homem, M. G. P.; Naves de Brito, A.; Wien, K.; da Silveira, E. F. *Earth, Moon Planets* **2005**, *97*, 311.
(27) Farenzena, L. S.; Collado, V. M.; Ponciano, C. R.; da Silveira, E. F.; Wien, K. *Int. J. Mass Spectrom.* **2005**, *243*, 85.
(28) Wien, K.; de Castro, C. S. C. *Nucl. Instrum. Methods B* **1998**, *146*, 178.
(29) Collado, V. M.; Farenzena, L. S.; Ponciano, C. R.; da Silveira, E. F.; Wien, K. *Surf. Sci.* **2004**, *569*, 149.
(30) Betts, R. L.; da Silveira, E. F.; Schweikert, E. A. *Int. J. Mass Spectrom.* **1995**, *145*, 9.
(31) Johnson, R. E. *Energetic Charged Particles Interaction with Atmospheres and Surfaces*; Springer-Verlag: Heidelberg, 1990.
(32) Woon, D. E. *Icarus* **2001**, *149*, 277.
(33) Lorenz, R. D.; Lunine, J. I. *Icarus* **1996**, *122*, 79.
(34) Martinez, R.; Ponciano, C. R.; Farenzena, L. S.; Iza, P.; Homen, M. G. P.; Naves de Brito, A.; Wien, K.; da Silveira, E. F. *Int. J. Mass Spectrom.* **2006**, *253*, 112.
(35) Nakai, H.; Goto, T.; Ichikawa, T.; Okada, Y.; Orii, T.; Takeuchi, K. *Chem. Phys.* **2000**, *262*, 201.
(36) Demaison, J.; Margules, L.; Boggs, J. E. *Chem. Phys.* **2000**, *260*, 65.

(37) Daigoku, K.; Miura, N.; Hashimoto, K. *Chem. Phys. Lett.* **2001**, *346*, 81.

(38) Wang, B. C.; Chang, J. C.; Jiang, J. C.; Lin, S. H. *Chem. Phys.* **2002**, *276*, 93.

(39) Martin, J. M. L.; Lee, T. J. *Chem. Phys. Lett.* **1996**, *258*, 129.

(40) Fernandez-Lima, F. A.; Ponciano, C. R.; da Silveira, E. F.; Chaer Nascimento, M. A. *Chem. Phys. Lett.* **2006**, *426*, 351.

(41) Fernandez-Lima, F. A.; Ponciano, C. R.; Chaer Nascimento, M. A.; da Silveira, E. F. J. *Phys. Chem. A* **2006**, *110*, 10018.

(42) McFarlane, R. D.; Torgerson, D. F. *Phys. Rev. Lett.* **1976**, *36*, 486.

(43) Cotter, R. J. *Time-of-Flight Mass Spectrometry: Instrumentation and Applications in Biological Research*; American Chemical Society: Washington, DC, 1997.

(44) Rosch, N.; Trickey, S. B. *J. Chem. Phys.* **1997**, *106*, 8940.

(45) Jaguar 6.0; Schrödinger Inc.: Portland, OR, 2004.

(46) Breneman, C. M.; Wiberg, K. W. *J. Comput. Chem.* **1990**, *11*, 361.